Identification of DNA methylation episignature for the intellectual developmental disorder, autosomal dominant 21 syndrome, caused by variants in the CTCF gene

Karimi, Karim; Mol, Merel O.; Haghshenas, Sadegheh; Relator, Raissa; Levy, Michael A.; Kerkhof, Jennifer; McConkey, Haley; Brooks, Alice; Zonneveld-Huijssoon, Evelien; Gerkes, Erica H.

Published in:
Genetics in Medicine

DOI:
10.1016/j.gim.2023.101041

Publication date:
2024

Genetics in Medicine (2024) 26, 101041

ELSEVIER

Genetics in Medicine
An Official Journal of the ACMG

www.journals.elsevier.com/genetics-in-medicine

ARTICLE

Identification of DNA methylation episignature for the intellectual developmental disorder, autosomal dominant 21 syndrome, caused by variants in the *CTCF* gene

Karim Karimi[1], Merel O. Mol[2], Sadegheh Haghshenas[1], Raissa Relator[1], Michael A. Levy[1], Jennifer Kerkhof[1], Haley McConkey[1], Alice Brooks[2], Evelien Zonneveld-Huijssoon[3], Erica H. Gerkes[3], Matthew L. Tedder[4], Lisenka Vissers[5], Emanuela Salzano[6], Maria Piccione[6,7], Sebastian Dorin Asaftei[8], Diana Carli[9,10], Alessandro Mussa[11], Elena Shukarova-Angelovska[12], Slavica Trajkova[9], Alfredo Brusco[9,13], Giuseppe Merla[14,15], Marielle M. Alders[16], Arjan Bouman[2,*], Bekim Sadikovic[1,17,*]

ARTICLE INFO

Article history:
Received 9 June 2023
Received in revised form
30 November 2023
Accepted 30 November 2023
Available online 3 December 2023

Keywords:
CTCF
Developmental disorder
DNA methylation
Episignature
IDD21

ABSTRACT

Purpose: The main objective of this study was to assess clinical features and genome-wide DNA methylation profiles in individuals affected by intellectual developmental disorder, autosomal dominant 21 (IDD21) syndrome, caused by variants in the CCCTC-binding factor (*CTCF*) gene.
Methods: DNA samples were extracted from peripheral blood of 16 individuals with clinical features and genetic findings consistent with IDD21. DNA methylation analysis was performed using the Illumina Infinium Methylation EPIC Bead Chip microarrays. The methylation levels were fitted in a multivariate linear regression model to identify the differentially methylated probes. A binary support vector machine classification model was constructed to differentiate IDD21 samples from controls.
Results: We identified a highly specific, reproducible, and sensitive episignature associated with *CTCF* variants. Six variants of uncertain significance were tested, of which 2 mapped to the IDD21 episignature and clustered alongside IDD21 cases in both heatmap and multidimensional scaling plots. Comparison of the genomic DNA methylation profile of IDD21 with that of 56 other neurodevelopmental disorders provided insights into the underlying molecular pathophysiology of this disorder.
Conclusion: The robust and specific CTCF/IDD21 episignature expands the growing list of neurodevelopmental disorders with distinct DNA methylation profiles, which can be applied as supporting evidence in variant classification.

Karim Karimi and Merel O. Mol contributed equally.

*Correspondence and requests for materials should be addressed to Bekim Sadikovic, Department of Pathology and Laboratory Medicine, Western University, 1151 Richmond St, London, Ontario N6A 3K7, Canada. *Email address:* bekim.sadikovic@lhsc.on.ca OR Arjan Bouman, Department of Clinical Genetics, Erasmus University Medical Center, Dr. Molewaterplein 40, 3015 GD, 2040, Rotterdam, 3000 CA, The Netherlands. *Email address:* a.bouman@erasmusmc.nl

Affiliations are at the end of the document.

doi: https://doi.org/10.1016/j.gim.2023.101041

Introduction

Neurodevelopmental disorders (NDDs) are a diverse group of conditions, including heritable disorders, which may affect up to 17% of the population.[1] These disorders are characterized by a range of complex and overlapping symptoms, which can make their clinical diagnosis challenging. Despite recent advancements in genomics and genetic testing, demonstrating an underlying genetic cause for many patients with suspected genetic disorders remains challenging. Traditional genetic tests may fail to detect a causal variant or identify genetic variants of uncertain clinical significance (VUS).[2]

DNA methylation of cytosine-guanine dinucleotides (CpGs) is an epigenetic modification with broad range of molecular functions including chromatin organization and gene expression.[3] The CpGs islands are a hotspot for pathological mutations across the human genome.[4] DNA methylation changes can be a functional consequence of variation in DNA sequences.[5] In recent years, specific patterns of the DNA methylation in over 50 distinct neurodevelopmental conditions, referred to as episignatures, have been validated as accurate biomarkers in clinical diagnostics.[5,6] Therefore, episignatures have been proven to be a useful diagnostic tool in the diagnostic assessment of patients with a suspected specific genetic syndrome, and in the reclassification of VUS detected using genomic sequencing or micro-array analysis.

Intellectual developmental disorder, autosomal dominant 21 (IDD21; MIM# 615502), is a syndromic condition characterized by developmental delay, intellectual disability, behavioral abnormalities, feeding difficulties, and, occasionally, minor facial dysmorphic features are also present. This NDD, which is also referred to as *CTCF*-related disorder, was first described by Gregor et al,[7] who reported 4 individuals with de novo variants in the CCCTC-binding factor (*CTCF*) gene. Since then, multiple case reports and larger patient cohorts have been published, expanding the genotypic and phenotypic spectrum of *CTCF*-related conditions.[8-14] Because of the atypical and heterogeneous phenotypes observed, the timely clinical diagnosis of this rare syndrome can be challenging.

This study describes the identification of a robust episignature for IDD21 established by analyzing the DNA from peripheral blood from a cohort of 16 patients with this syndrome. Two clinical examples are provided in which the episignature biomarker eventually led to a diagnosis of IDD21 syndrome. We also compared the IDD21 methylation signature and performed functional and correlative assessment of DNA methylation patterns, relative to other established episignature disorders. This study demonstrates the clinical utility of IDD21 episignature, as part of the growing number of episignature disorders, in clinical genetic practice.

Materials and Methods

Subjects and cohorts

DNA samples were extracted from peripheral blood of 16 individuals (age range 3-37 years; 9 males and 7 females) with genetic variants in *CTCF* and clinical features consistent with IDD21. Supplemental Table 1 presents the clinical features and genetic variants classified as pathogenic, likely pathogenic, and VUS according to American College of Medical Genetics (ACMG) and the Association for Molecular Pathology (AMP) guidelines.[15,16] The transcript number NM_006565.3 was used for the *CTCF* variants analysis. Ten subjects had certain pathogenic or likely pathogenic heterozygous variants, whereas 6 VUS were identified in 6 unrelated individuals.

The samples with pathogenic or likely pathogenic variants were divided into 2 cohorts: 7 samples were used as discovery cohort, and 3 remaining samples were then used to validate the IDD21 epsignature. The discovery cohort was used to select probes and construct the model. We then applied the IDD21 epsignature to VUS samples and assessed them using supervised and unsupervised clustering methods. Finally, all the samples, including the now reclassified pathogenic cases with previous VUS findings, with a confirmed IDD21 epsignature were used to train the model and to perform functional analysis.

All the samples and records were de-identified. Physicians obtained written consent from the patients for use of their clinical information in this research. The research was conducted in accordance with all relevant ethical regulations. The study protocol was approved by the Western University Research Ethics Board (REB 106302).

Methylation data analysis

DNA methylation analysis was performed using the Illumina Infinium Methylation EPIC Bead Chip microarrays according to the manufacturer's protocol (Illumina). This array type covers more than 860,000 CpG sites across the human genome. The procedure of DNA methylation analysis and episignature discovery were previously described.[6,17] The intensity data files including the methylated and unmethylated signal intensities were analyzed using R 4.2.0. The minfi package (version 1.42.0) was used to normalize the data using the Illumina normalization method with background correction.[18] Probes with detection P value $> .01$ and those located on X and Y chromosomes were excluded. In addition, probes containing single-nucleotide variations (formerly single-nucleotide polymorphisms) at or near the CpG interrogation or single nucleotide extension sites, as well as those cross-reacting with chromosomal locations other than their target regions were discarded from the data set. In total, 689,325 probes remained for further analyses. Moreover, arrays

having high probe failure (>5%) and those imposing the batch effect were excluded from the data set. The genome-wide methylation density was assessed for all the samples to exclude those deviating from a bimodal signal distribution. The structure of batches was assessed using principal component analysis (PCA) to identify outliers.

Selection of matched controls

Controls were randomly selected from EpiSign™ Knowledge Database (EKD)[19] at the London Health Sciences Centre. Controls were matched based on age, sex, and array type using MatchIt package (version 4.5.1).[20] The matching quality and sample sizes were optimized to achieve consistency across all analyses. For each matching trial, PCA was performed to ensure none of the matched controls were outliers. This process was repeated until no outlier could be identified by the PCA's first 2 components. The final sample size of controls ($n = 56$) was 8 times larger the size of cases included in the discovery cohort ($n = 7$).

DNA methylation profiling of IDD21

Methylation level (β-value) of each probe was calculated as the ratio of methylated signal intensity over the sum of methylated and unmethylated signal intensities, ranging between 0 (no methylation) and 1 (full methylation). The β-values were then logit transformed into M-values ($\log_2(\beta/(1-\beta))$) to increase the homoscedasticity for linear modeling. The M-values were fitted in a multivariate linear regression model using the limma package (version 3.52.4)[21] to identify the differentially methylated probes (DMPs). The model was adjusted for confounding variable of blood cell type composition. The blood cell type mixture was estimated based on the algorithm developed by Houseman et al.[22] The eBayes function of the limma package was applied to moderate the P values obtained in linear modeling. In addition, the P values were corrected for multiple testing according to the Benjamini and Hochberg method.[23] The best set of probes was selected in 3 steps. Initially, the absolute methylation difference between cases and controls were multiplied by the negative value of the log-transformed adjusted P value, and 800 probes with the highest scores were selected for the next step. At the second step, a receiver's operating curve characteristics analysis was applied to choose 400 probes with the highest area under the receiver's operating curve. Finally, the pairwise correlation coefficient of probes were measured between case and control samples, and 159 probes with correlation >.90 were removed. The remaining 241 DMPs were then used to construct a hierarchical clustering (heatmap) model using Ward's method on Euclidean distance. Furthermore, a multidimensional scaling (MDS) model was performed by scaling of the pairwise Euclidean distances between samples to evaluate separation between the cases and controls.

Construction of a classification model

A binary support vector machine (SVM) classification model was trained using the e1071 R package (version 1.7-13), as previously described.[6,19] The classifier generates a methylation variant pathogenicity (MVP) score predicting the probability that a sample's methylation pattern matches a given episignature. The MVP scores range between 0 and 1, with scores close to 1 indicating a high probability of a methylation pattern for the target syndrome and scores close to 0 indicating a methylation profile similar to controls. Training cases, matched controls, 75% of other controls and 75% of cases of 56 other NDDs from the EKD were used to train the SVM classifier. The remaining 25% of controls and 25% of other NDDs from the EKD were used for testing. The SVM classifier was generated in different analyses including episignature discovery, validation of IDD21 episignature, and assessment of VUS samples. The final model was trained using 12 samples with a confirmed IDD21 episignature.

Cross validation

The robustness of the episignatures was assessed using 12 rounds of leave-one-out cross validation. In each round, 11 of samples with a confirmed IDD21 episignature were used for probe selection and the other one was included as testing sample. The heatmap and MDS plots were used to visualize the samples classification in each round.

Functional annotation and comparison of IDD21 to other episignature syndromes

Functional annotation was performed according to the procedure that was previously described by Levy et al.[24] To assess the overlap between the methylation profile of IDD21 and other disorders, the IDD21 subjects were trained against controls matched for age and sex. The controls were selected from individuals who were not diagnosed with a disorder or did not have an identified episignature. Probes with mean methylation differences >5% between the IDD21 cases and the matched controls, and Benjamini and Hochberg adjusted P values < .01 were selected as DMPs. Heatmap and circus plots were used to visualize the percentage of DMPs shared between IDD21 and 56 other NDDs in the clinical EKD. Heatmap and circos plots were generated using pheatmap (version 1.0.12) and circlize (version 0.4.15)[25] R packages, respectively. The top 500 DMPs with the most significant P values were used to measure the distance and similarities between IDD21 and other 56 EKD cohorts using clustering methods. The global methylation differences and total number of identified DMPs in each cohort were visualized by a tree and leaf plot using the R package TreeAndLeaf (version 1.6.1).

Identification of the differentially methylated regions of IDD21

The differentially methylated regions (DMRs) were identified using the DMRcate package (version 2.10.0) in R.[26] A region was considered as DMR if it harbors at least 5 different CpGs within 1 kb with a minimum methylation difference of 10% between the case and the control samples, and a Fisher's multiple comparison P value < .01. The annotatr R package (version 1.22.0) was used to annotate the genomic locations of DMRs with CpG islands (CGIs) and genes.[27] The annotations hg19_cpgs, hg19_basicgenes, hg19_genes_intergenic, and hg19_genes_intronexonboundaries within the AnnotationHub (version 3.2.2) were used as annotation resources. The CGI annotations included CGI shores, which encompassed 0-2 kb on either side of CGIs, CGI shelves, which encompassed 2 to 4 kb on either side of CGIs, and inter-CGI regions, which covered all remaining regions. The genomic regions within 1 kb upstream of the transcription start site were classified as promoters, and regions from 1 to 5 kb upstream of the transcription start site were classified as promoter+. Untranslated regions (5'-UTR and 3'-UTR), exons, introns, and exon/intron boundaries were included in gene annotations under the "gene body" category. The gene ontology (GO) analysis was then performed on detected DMRs using missMethyl (version 1.28.0) package of R.[28]

Results

The case cohort included 16 subjects, including 10 with a pathogenic or likely pathogenic heterozygous variant in the *CTCF* gene, and 6 with a VUS. Fourteen individuals carried missense variants, whereas 2 subjects had a non-sense variant. All patients presented with clinical features consistent with those previously described as associated with IDD21, including intellectual disability/developmental delay, autism, and variable structural anomalies. Supplemental Table 1 presents the molecular, demographic, and clinical features of all included individuals. The molecular details, including de novo and previously identified *CTCF* variants, are presented in Supplemental Figure 1. Five novel variants, including case 5 (p.Arg339Leu), case 11 (p.His541Leu), case 12 (p.Leu98Ser), case 13 (p.Pro200Ser), and case 14 (p.Ile685Met), were reported for the first time.

Identification and assessment of an episignature for IDD21

Discovery of IDD21 episignature

Seven samples with pathogenic or likely pathogenic variants were initially used for probe selection and model construction. A clear separation was observed between cases and controls in both hierarchical clustering (heatmap), and MDS plots, confirming that selected probes were able to distinguish the IDD21 cases from controls (Supplemental Figure 2A and B). In addition, all training cases obtained an MVP score close to 1, confirming the similarity of the detected methylation pattern to the IDD21 episignature. MVP scores were close to 0 for all testing samples from the other NDDs, indicating the full specificity of the classifier (Supplemental Figure 2C).

Validation of IDD21 episignature

We then used the 3 remaining samples with pathogenic or likely pathogenic variants (cases 4, 9, and 10) to validate the IDD21 episignature. All 3 testing samples were clustered alongside the cases in heatmap and MDS plot (Figure 1A and B). Furthermore, an MVP score >0.5 was observed for all 3 validation samples, confirming the similarity of the detected methylation patterns to the IDD21 episignature (Figure 1C). These 3 samples with a confirmed episignature were then added to training cohort for further analyses.

Assessment of VUS samples

We used the 6 VUS samples as testing set and assessed them using supervised and unsupervised methods. This analysis indicated that 2 VUS samples (cases 11 and 12) mapped to the episignature, and clustered with IDD21cases in both heatmap and MDS plots (Figure 2A and B). However, 4 other VUS samples did not match to the episignature and clustered alongside the controls. This analysis confirmed that the IDD21 episignature can be used to re-classify VUS samples. Two positive VUS samples were then added to training set to construct the classifier.

Final classification

All the samples with a confirmed episignature ($n = 12$) were used to train the model and to construct the classifier. The methylation β-values were compared with controls matched for age, sex, and array type, with a case to control ratio of 1:5. In total, 226 differentially methylated CpG probes were selected for the IDD21 discovery episignature with mean methylation differences of 12% to 38% (Supplemental Table 2). Hierarchical clustering (heatmap) confirmed that the selected probes were able to distinguish the IDD21 cases from the matched controls (Figure 3A). In addition, a clear separation was observed between cases and controls using MDS plot (Figure 3B), demonstrating the robustness of the episignature. The SVM model was constructed using the 226 selected DMPs to differentiate IDD21 samples from controls. The SVM classifier was trained using 12 cases and 60 matched controls along with 75% of other controls and 75% of cases from 56 other NDDs from the EKD. The remaining 25% of controls and 25% of other disorders from the EKD were used as testing set. This model demonstrated

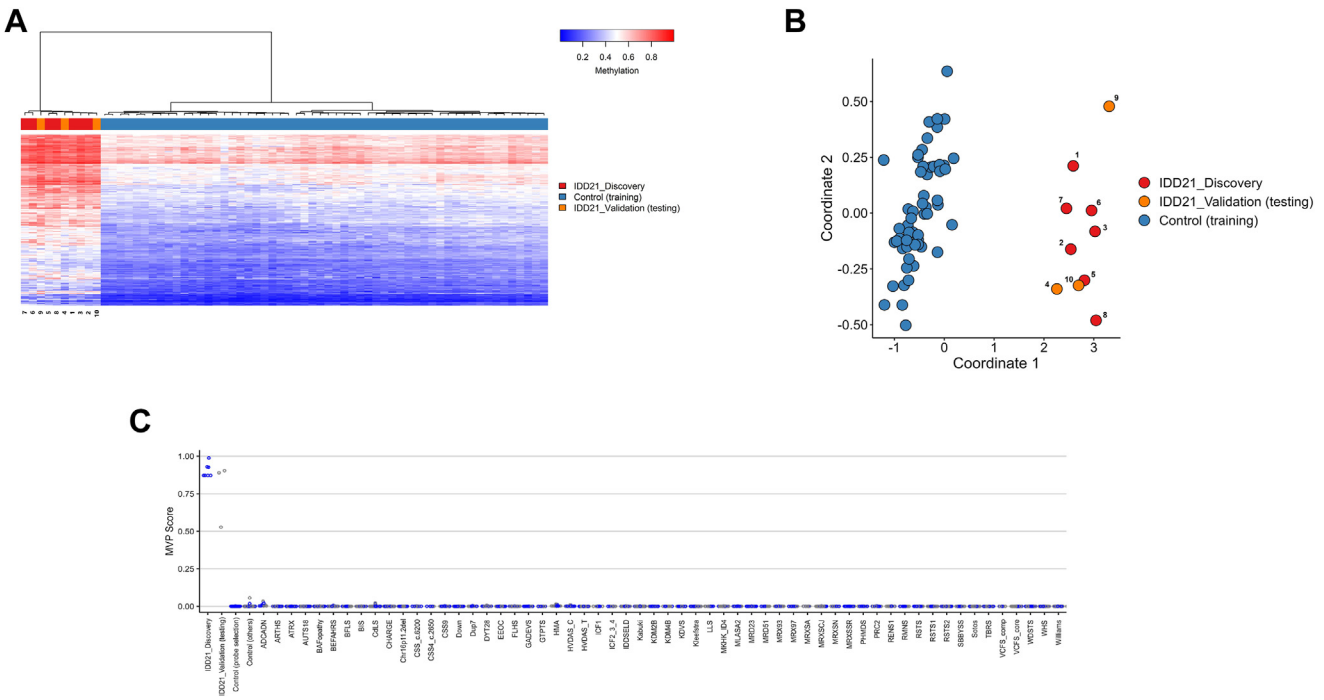

Figure 1 Validation of IDD21 (*CTCF* gene) episignature. A. Euclidean hierarchical clustering (heatmap): each column presents a single IDD21 case or control, and each row represents one of 237 probes selected for episignature discovery. A clear separation was observed between cases (red) and controls (blue). Three samples were used as validation set (orange), all of them were clustered with IDD21 cases. B. Multidimensional scaling (MDS) plot presents the differentiation between cases (red) and controls (blue). Three samples were used as validation set (orange), all of them were clustered with IDD21 cases. C. Support vector machine (SVM) classifier: the model was trained by comparing the cases with 75% of controls and 75% of the other 56 neurodevelopmental disorders (blue circles). The remaining 25% of controls and 25% of the other 56 neurodevelopmental disorders were used for testing (gray circles). Three validation samples provided MVP scores >0.5, confirming their similarity to IDD21 episignature.

that all testing samples from other NDDs show an MVP score close to 0, confirming full specificity of the model (Figure 3C). The reproducibility and sensitivity of episignature were further assessed using 12 rounds of leave-one-out cross validation. The resulting heatmap and MDS plots indicated that all tested cases were correctly clustered with the training cases in each round of cross validation (Supplemental Figure 3).

The IDD21 episignature can be used to classify unresolved samples

We applied the IDD21 episignature to the EKD which includes thousands of genome-wide DNA methylation profiles from individuals with known episignature syndromes, as well as thousands of previously assessed, unresolved individuals with suspected genetic conditions. We identified 2 samples with high MVP scores in the SVM classifier that were previously unresolved clinical cases (Unresolved column in Figure 3C). Heatmap and MDS plots also demonstrated that these samples were clustered with IDD21 cases (Supplemental Figure 4). For both cases, the clinical providers confirmed the presence of clinical features matching IDD21. A likely pathogenic CTCF variant, c.1033C>T p.(His345Tyr), was identified in 1 case. CTCF sequencing data were not available for the second case. No false-positive cases were found among the analyzed samples. These results further confirmed robustness and clinical utility of this classifier and that IDD21 episignature can be used for screening and identification of patients with IDD21 and simultaneously provide functional evidence for genetic variant classification.

Functional mapping and correlative analysis of the IDD21 episignature and 56 EpiSign v3 classifier disorders

The IDD21 samples were compared with matched controls from the EKD to explore DMPs. This analysis was performed using controls unaffected by a neurodevelopmental condition or NDD subjects without a known episignature. We compared the number of DMPs for the IDD21 cohort with those previously reported for 56 other neurodevelopmental cohorts included in EpiSign v3 classifier on the EKD (Figure 4). The list of disorders and their abbreviations are presented in Supplemental Table 3. The total number of 4558 DMPs were recognized for IDD21 with the range of 279 to 151,848 DMPs among other disorders from the EKD. The IDD21 cohort had the highest percentage of overlap with HVDAS_C

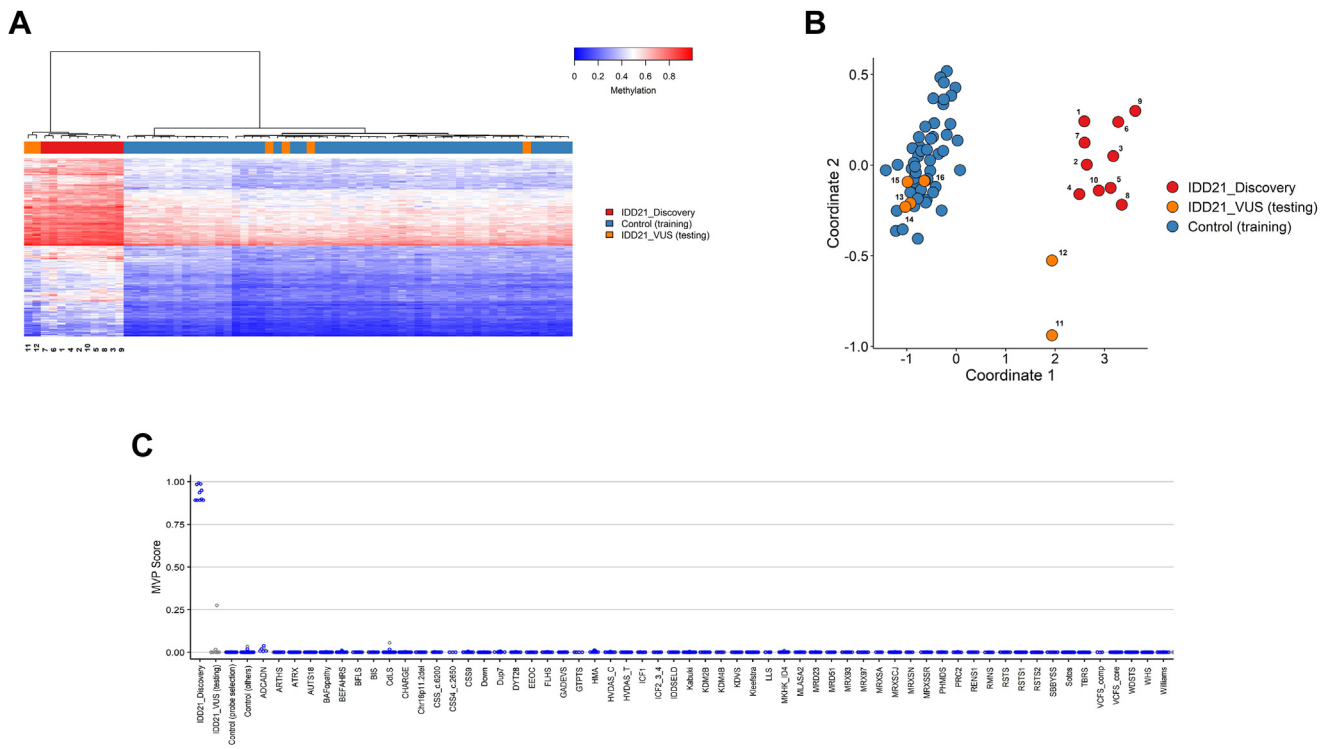

Figure 2 **Assessment of VUS sample.** A. Euclidean hierarchical clustering (heatmap): each column presents a single IDD21 case or control, and each row represents 1 of 273 probes selected for episignature discovery. A clear separation was observed between cases (red) and controls (blue). VUS samples were used as testing set (orange): 2 of VUS were clustered alongside the IDD21 cases. B. Multidimensional scaling (MDS) plot presents the differentiation between cases (red) and controls (blue). The VUS samples were used as testing set (orange): 2 of VUS were clustered with IDD21 cases. C. Support vector machine (SVM) classifier: the model was trained by comparing the cases with 75% of controls and 75% of the other 56 neurodevelopmental disorders (blue circles). The remaining 25% of controls and 25% of the other 56 neurodevelopmental disorders were used for testing (gray circles).

(14%) and HVDAS_T (11%), respectively. Both aforementioned episignatures are related to Helsmoortel-van der Aa syndrome (HVDAS) caused by variants in the activity-dependent neuroprotector homeobox (*ADNP*) gene, where HVDAS_C is associated with variants in central domains, whereas HVDAS_T encompass variants within the terminal domain.

The mean of β-values differences was compared between the IDD21 cohort and 56 other NDDs (Figure 5). The overall methylation trend confirmed the predominant hypermethylation changes for IDD21 cohort. The relatedness of genome-wide methylation profiles in all cohorts was assessed using clustering method. The top 500 DMPs from each cohort were used in this analysis. This analysis confirmed that the IDD21 is closely clustered with HVDAS_C (*ADNP* gene) episignature (Figure 6).

DMRs

In total, 21 DMRs were detected using the DMRcate algorithm. This analysis confirmed that all identified DMRs were hypermethylation events (Table 1). The locations of DMRs were then annotated in relation to CGIs and genes. This analysis revealed that the DMRs are mainly found in CGIs (67%) and Inter_CGI (24%), respectively (Figure 7A). In addition, the annotation analysis indicated that the highest percentages of DMRs were in coding sequence (47%) and promoter regions (33%), respectively (Figure 7B). The GO enrichment analysis revealed 24 significant GO terms (P value < .01), which were mostly related to *FLOT1* (MIM# 606998), *ATF6B* (MIM# 600984) and *HEYL* (MIM# 609034) genes (Supplemental Table 4). Notch signaling, skeletal muscle tissue development, and positive regulation of synaptic transmission are the significant GO terms, which might be relevant to IDD21 features.

Discussion

The aim of this study was to assess the evidence for a possible DNA methylation episignature for individuals with the *CTCF*-related condition, IDD21. For this purpose, we assessed the DNA methylation profiles of 16 individuals carrying different types and ACMG/AMP classes of *CTCF* variants. We demonstrated that the aberrant methylation changes represent a highly specific, reproducible, and sensitive biomarker, supporting the molecular diagnosis of IDD21. Considering the variable phenotypic presentation of the syndrome,[13] also exemplified by our clinically heterogeneous cohort, establishing the diagnosis purely on the basis of

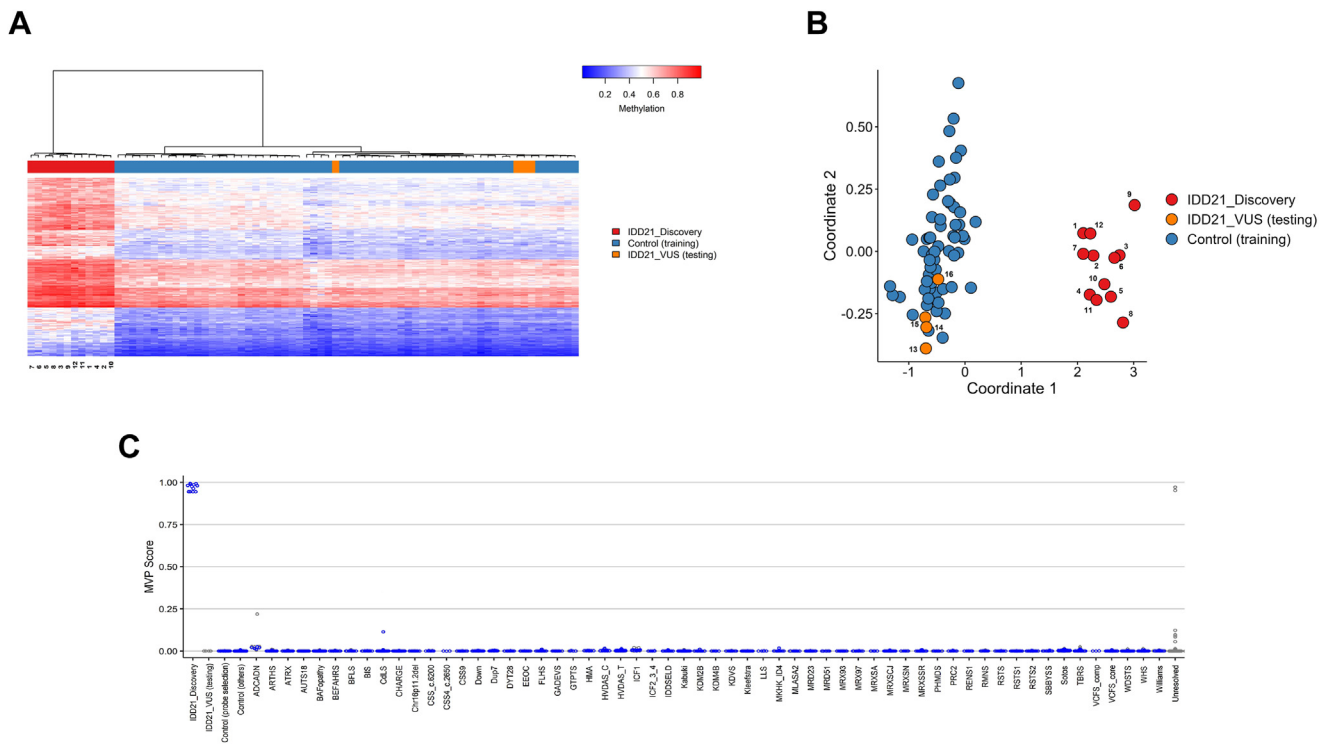

Figure 3 Final classification of all cases with a confirmed IDD21 episignature. A. Euclidean hierarchical clustering (heatmap): each column presents a single IDD21 case or control, and each row represents 1 of 226 probes selected for episignature discovery. A clear separation was observed between cases (red) and controls (blue). Four VUS samples did not map to IDD21 episignature (orange). B. Multidimensional scaling (MDS) plot presents the differentiation between cases (red) and controls (blue). Four VUS samples did not map to IDD21 episignature (orange). C. Support vector machine (SVM) classifier: the model was trained by comparing the cases with 75% of controls and 75% of the other 56 neurodevelopmental disorders (blue circles). The remaining 25% of controls and 25% of the other 56 neurodevelopmental disorders were used for testing (gray circles). The IDD21 samples provided MVP scores close to 1, indicating the high specificity of the classifier.

clinical features can be challenging. Our results confirm that the IDD21 episignature can be applied as an effective diagnostic tool. This was further illustrated by screening thousands of profiles from unresolved cases with a suspected genetic condition, leading to the identification of 2 novel cases harboring likely pathogenic variants in *CTCF*. Subsequent follow-up with the clinical providers, including review of exome sequencing data, confirmed a likely pathogenic variant (c.1033C>T p.(His345Tyr)), in 1 of the cases.

CTCF (CCCTC-binding factor) is a highly conserved protein involved in gene expression regulation and chromatin architecture. Because of distinct combinations of its 11 zinc-finger domains, enabling interactions with ~50,000 binding sites across the genome, it is implicated in a myriad of genomic regulatory processes, including the formation of chromatin domains,[29] genomic imprinting,[30] X chromosome inactivation,[31] and alternative splicing.[32] The CTCF binding sites are sensitive to DNA methylation, linking the widespread occupancy of CTCF to specific methylation patterns.[33,34] Indeed, perturbed DNA methylation has been shown previously in patients with a *CTCF* microdeletion.[9] Our discovery of a specific *CTCF* episignature is consistent with these earlier observations. Additionally, 2 patients (cases 6 and 7) carrying the identical *CTCF* variant (c.1699C>T p.(Arg567Trp)) displayed the oncological phenotypes. Case 7 has a secondary finding in *PTPN11* (MIM# 176876) responsible for juvenile myelomonocytic leukemia, and case 6 was diagnosed with rhabdomyosarcoma. These findings further support the significant involvement of *CTCF* in the development of various types of cancer, as also previously shown by tissue-specific methylation patterns at CTCF binding sites among different tumor types.[35,36]

Equally important, we showed that the episignature can be utilized to assess the pathogenicity of novel variants. The patient cohort included 6 individuals with a VUS. The methylation profiles of 2 subjects clearly mapped with the episignature, demonstrating strong functional evidence, thereby enabling reclassification of these variants to likely pathogenic. Although the other 4 samples clustered with the controls, interpretation of pathogenicity in these variants requires further investigation. CTCF's functions extend beyond its sensitivity to DNA methylation patterns because it also actively interacts with RNA and other proteins, eg, cohesion.[37] Therefore, the episignature may not be sufficient by itself to accurately classify the *CTCF* variants. For

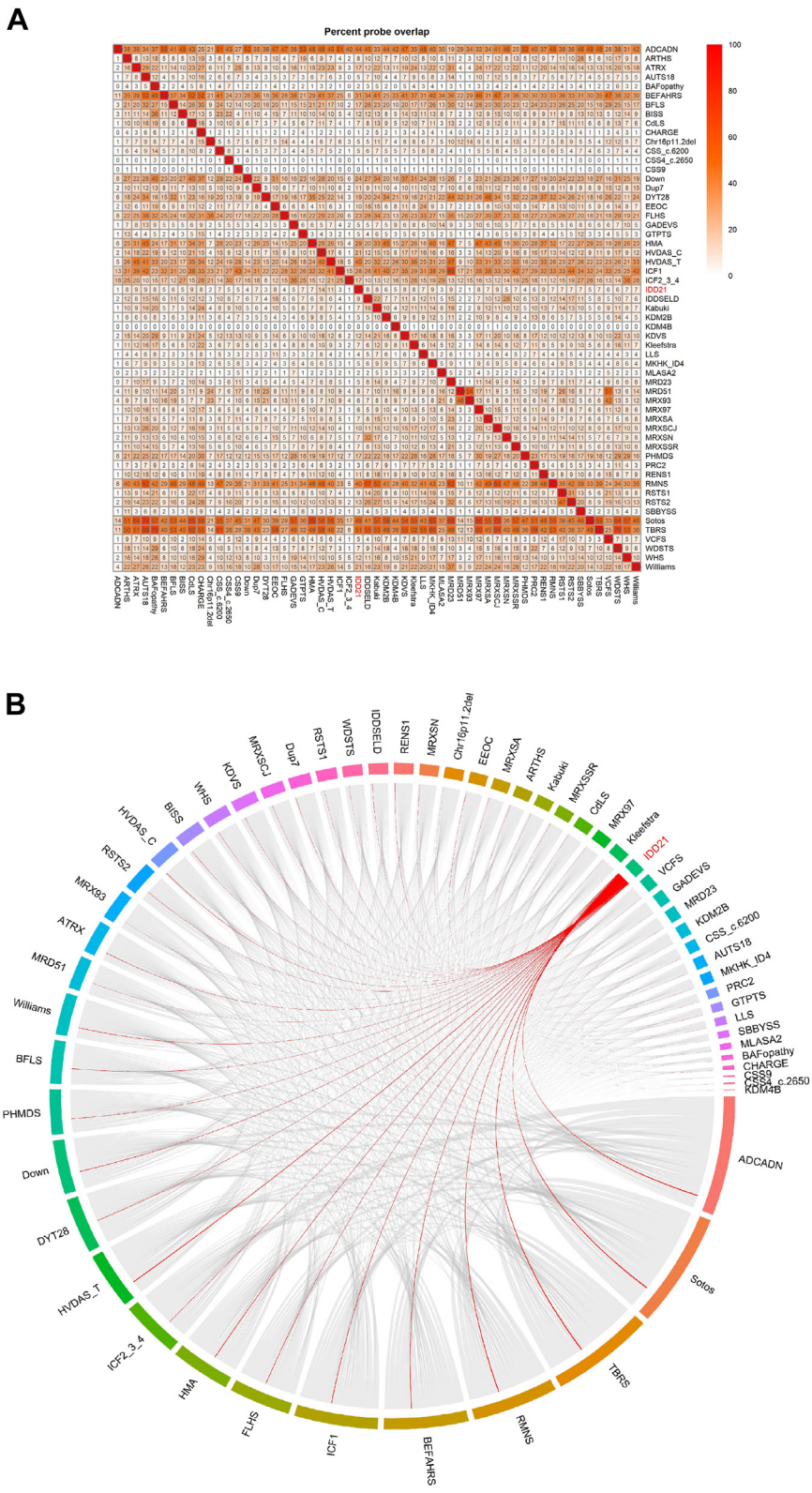

Figure 4 Differentially methylated probes (DMPs) shared between IDD21cohort and the 56 other neurodevelopmental disorders from EKD. A. Heatmap presenting the percentage of probes shared between each pair of cohorts. Colors show the percentage of *y*-axis cohort's probes shared with the *x*-axis cohort's probes. B. Circos plot showing the probes shared between each pair of cohorts. Abbreviations are provided in Supplemental Table 3.

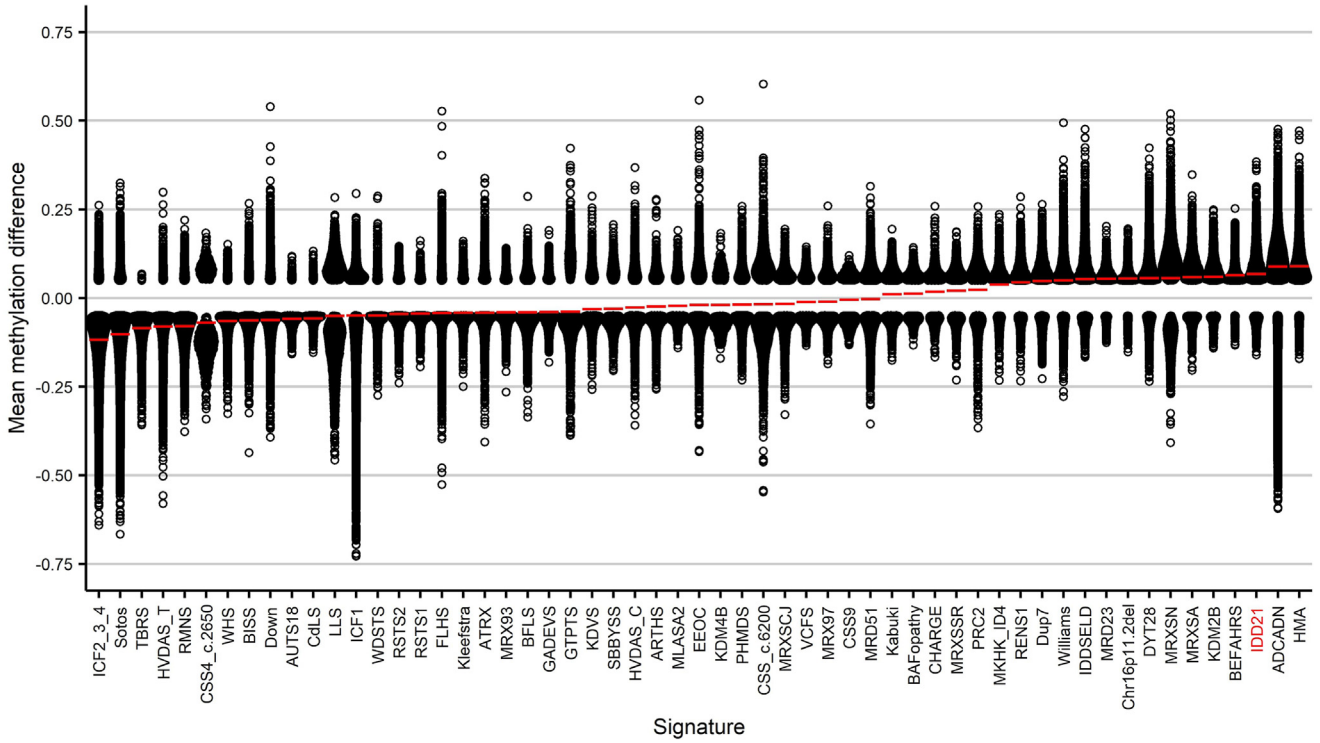

Figure 5 **Methylation differences of all differentially methylated probes for each cohort.** Red lines indicate mean methylation. Each circle represents 1 probe. An overall hyper-methylation trend was observed in IDD21cohort.

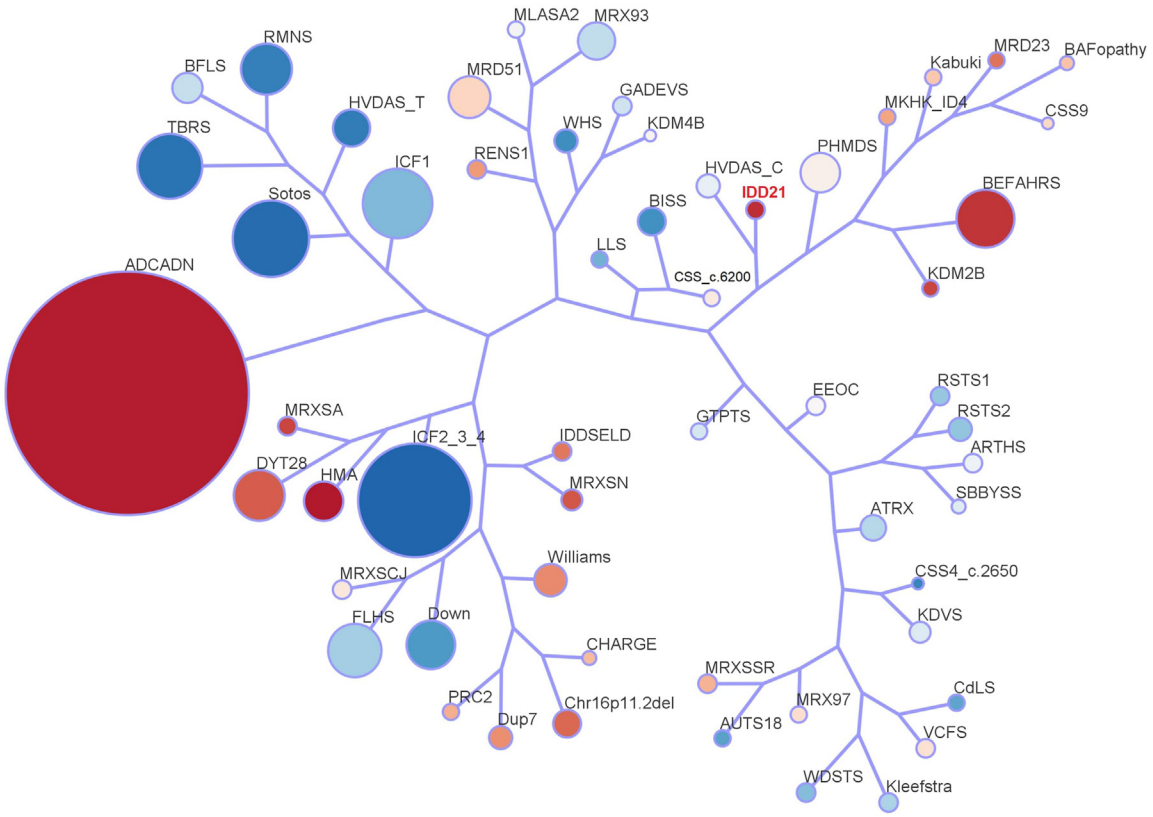

Figure 6 **Tree and leaf plot of Euclidean clustering of all 56 cohorts using the top DMPs for each cohort.** A leaf node represents a cohort, with node sizes illustrating relative scales of the number of selected DMPs for the corresponding cohort, and node colors are indicative of the overall mean methylation difference. Abbreviations are listed in Supplemental Table 3.

Table 1 List of differentially methylated regions (DMRs) for the IDD21 cohort. Computations were based on hg19 reference genome and annotation

Chromosome	Start	End	Number of CpGs	Mean Methylation Difference	Overlapping Genes
chr6	32,085,541	32,087,190	16	0.11	*ATF6B*
chr6	30,698,584	30,699,481	11	0.17	*FLOT1*
chr12	56,074,329	56,075,511	7	0.10	*METTL7B*
chr1	2,063,799	2,064,765	6	0.13	*PRKCZ*
chr2	240,868,184	240,868,631	5	0.12	*NDUFA10*
chr19	44,039,475	44,040,457	5	0.13	*ZNF575*
chr18	74,535,233	74,536,226	7	0.11	*ZNF236*
chr1	40,105,079	40,105,706	6	0.11	*HEYL*
chr12	133,177,075	133,178,316	8	0.12	-
chr19	11,517,079	11,517,436	5	0.17	*RGL3*
chr6	25,732,146	25,733,243	5	0.12	*HIST1H2APS1, HIST1H2BPS1*
chr2	98,928,364	98,928,898	5	0.10	*VWA3B*
chr19	17,877,419	17,877,846	6	0.11	*FCHO1*
chr13	113,689,139	113,689,955	5	0.10	*MCF2L*
chr19	1,795,638	1,796,985	5	0.11	*ATP8B3*
chr21	43,198,283	43,198,797	6	0.10	-
chr10	101,824,920	101,825,185	5	0.10	*CPN1*
chr8	43,131,260	43,132,451	6	0.13	*RP11-726G23.10*
chr5	23,506,738	23,507,656	6	0.11	*PRDM9*
chr17	20,799,408	20,799,532	5	0.10	*RP11-344E13.3, CCDC144NL*
chr10	134,043,362	134,043,897	6	0.10	*STK32C*

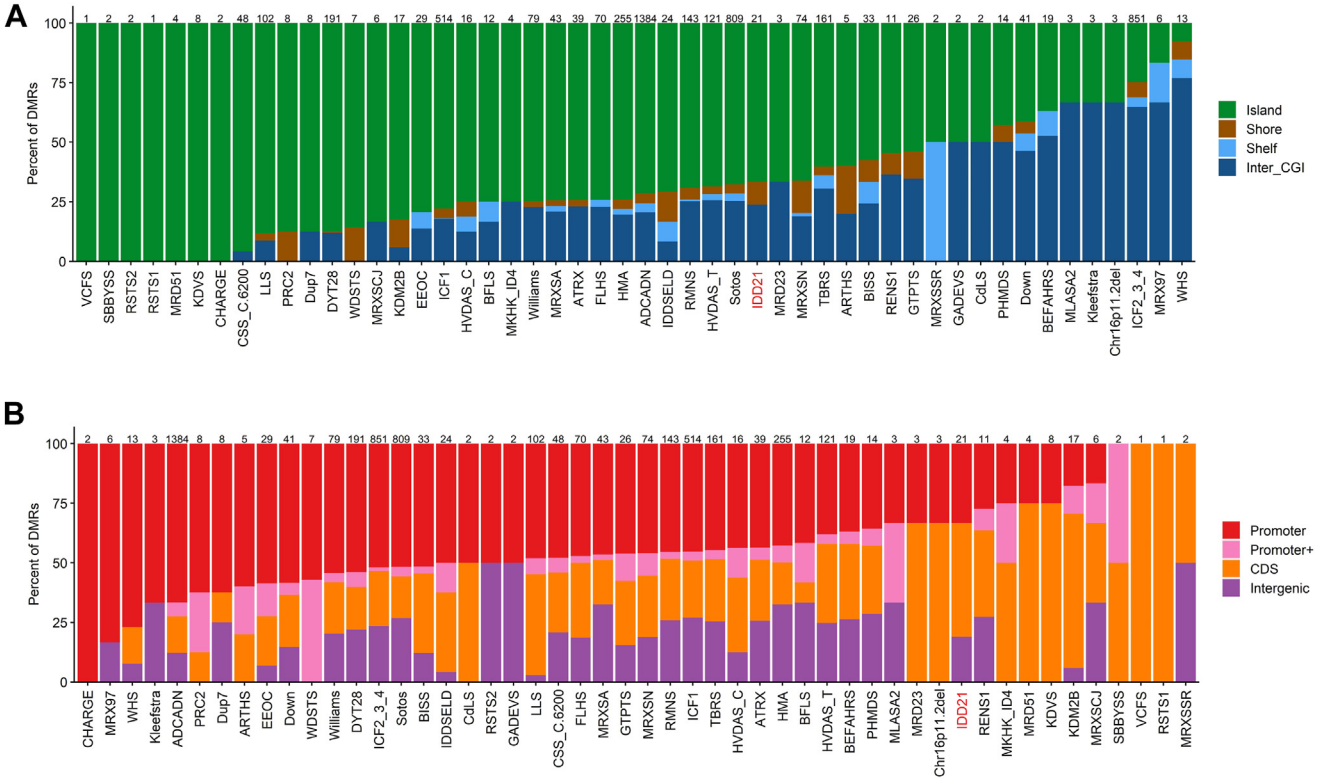

Figure 7 **Differentially methylated regions (DMRs) annotated in relation to CpG islands and gene.** A. DMRs annotated in the context of CpG islands, including CpG islands (Island), within 0 to 2 kb of a CpG island boundary (Shore), within 2 to 4 kb of a CpG island boundary (Shelf), and all other regions in the genome (Inter_CGI). B. DMRs annotated in the context of genes including 0 to 1 kb upstream of the transcription start site (Promoter), 1 to 5 kb upstream of the transcription start site (Promoter+), coding sequence (CDS), and all other regions of the genome (Intergenic). Abbreviations of all cohorts were listed in Supplemental Table 3.

example, the p.(Arg278Leu) variant is located in the zinc finger 1 domain, which displays distinct structural characteristics compared with other domains. Although structural data indicate a potential absence of DNA recognition/binding function in this terminal zinc finger 1, computational modeling shows that this variant introduces a hydrophobic residue on the surface, likely significant for non-DNA interactions.[38] Consequently, the effect of this variant may not be fully explained by methylation disturbances alone, and other non-DNA interactions should be considered to understand its overall impact. In addition, although the central zinc-finger domains of *CTCF* serve as the DNA binding sites, the N and C termini interact with protein partners, facilitating loop extrusion and other functions.[39] Therefore, these specific regions might be related to distinct DNA methylation profiles or influenced by other non-methylation regulatory factors. This study observed a limited number of variants within the N and C termini of *CTCF*, suggesting further research to explore a broader range of variants in the future. Besides these 4 VUS, we identified a uniform methylation pattern among the 11 distinct *CTCF* variant types and positions (Supplemental Figure 1).

Given the ubiquitous and versatile roles of *CTCF*, one might expect to find overlap with other episignature disorders. In our comparative analysis with other established episignatures, we observed the highest overlap with patients affected by HVDAS, a rare neurodevelopmental condition caused by variants in the *ADNP*.[40,41] Clinically, HVDAS and IDD21 share multiple features, such as mild to severe intellectual disability, autism, behavioral disturbances, hypotonia, feeding difficulties, and congenital cardiac defects.[13,41] This might imply that the 2 syndromes share a molecular background, although it must be noted that partial clinical overlap is seen with other genetic syndromes as well (eg, Coffin-Siris, Kleefstra, and Smith-Magenis syndromes). On a molecular level, *ADNP* (MIM# 611386) may regulate gene expression directly as transcription factor or indirectly by association with *BRG1* (MIM# 603254), *CHD4* (MIM# 603277), and *CTCF* as genome organizers.[42,43] Transcriptome analysis of *CTCF*-affected individuals showed a moderate decrease of *ADNP* blood expression levels ($\log_2$ fold change: −0.79).[14] These observations may reflect the interaction between *ADNP* and *CTCF*, underlying the partial overlap in episignatures across the 2 conditions, although this needs to be validated in larger cohorts and on a functional level. In future studies, it would also be interesting to assess whether other genetic conditions related to CTCF targets show an overlapping methylation profile, which might provide clues toward molecular etiologies.

Finally, we noted that the all DMRs were hypermethylation events, which is in line with gene expression profiles of predominantly downregulated genes in *CTCF*-affected individuals.[14] Further analysis indicated that the DMRs encompass several genes related to NDDs and DNA methylation mechanisms. For example, the DMR found on chromosome 1 involves the *PRKCZ* (MIM# 176982), which has been identified as 1 of the genes associated with chromosome 1p36 deletion syndrome.[44] This syndrome is a chromosome disorder causes severe intellectual disability, poor growth with microcephaly, dysmorphic facial features, and axial hypotonia.[45] The *PRKCZ* hypermethylation also plays a critical role in *CTCF* deletion syndrome.[9] Konrad et al[14] reported a modest increase in *PRKCZ* expression (log2 fold change: 0.56) in the blood transcriptomic analysis of *CTCF* patients. However, it is anticipated that the interplay and role of *PRKCZ* in the IDD21 occurs at the brain level, warranting further investigation in the brain-specific contexts. The DMR identified on chromosome 6 coincided with the *FLOT1* (MIM# 606998), which is involved in the formation of glutamatergic synapses in hippocampal neurons and has been linked to neurodegenerative disorders.[46,47] The DMR located on chromosome 2 involves *VWA3B* (MIM# 614884), which cause cerebellar ataxia with intellectual disability.[48] In addition, the *HEYL* (MIM# 609034) was found on DMR of chromosome 1, which is suggested to promote neuronal differentiation of neural progenitor cells.[49] Additionally, Konrad et al[14] reported altered gene expression levels for *ZNF236* (MIM# 604760) (log2 fold change: −1.02), *ZNF575* (HGNC# 27606) (log2 fold change: 0.89), and *RGL3* (MIM# 616743) (log2 fold change: −1.29), which were among those genes identified as part of the DMRs in this study. Furthermore, the DMR overlapping with *ATP8B3* (MIM# 605866) (chr19: 1,795,638-1,796,985) exhibited significant CTCF peaks, as revealed by the ChIP-seq data retrieved from the Encyclopedia of DNA Elements (ENCODE) database (ENCFF067QSR) (Supplemental Figure 5). Although these data suggest some overlaps between functional genomic profiles of CTCF and the DMRs highlighted in this study, future in-depth and functional evaluation of these genes is essential to provide deeper insights on *CTCF*-related disease mechanism through its activating role on target genes and downstream pathways.

Conclusion

The development of a robust and specific *CTCF*/IDD21 epigenetic signature adds a novel member to the growing list of NDDs with distinct DNA methylation profiles, which can be applied in screening and diagnosis, as well as in the classification of novel ambiguous variants. Besides optimizing diagnostic capabilities, our results illustrate that episignatures might also be leveraged to simultaneously provide further insight into pathophysiological mechanisms by comparison with other episignatures and through exploration of affected methylated regions. Further functional analyses are necessary to increase our understanding of the underlying molecular etiologies, potentially leading to the identification of therapeutic targets.

Data Availability

Data sets used in this study that are available publicly are previously described.[19] Anonymized data for each subject are described in the study. The individual genomic and epigenomic or any other personally identifiable data for other samples in the EpiSign Knowledge Database are prohibited from deposition in publicly accessible databases because of institutional and ethics restrictions. Specifically, these include data and samples submitted from external institutions to London Health Sciences EpiSign Knowledge Database that are subject to Institutional Material and Data Transfer agreements, data submitted to London Health Sciences for episignature assessment under Research Services Agreements, and research study cohorts under Institutional Research Ethics Approval (Western University REB 106302; and REB 116108). Some of the software packages used in this study are publicly available as described in the Materials and Methods. EpiSign is a commercial software and is not publicly available.

Acknowledgments

The authors are grateful to patients and their families for their participation in this study.

Funding

Funding for this study is provided in part by the Government of Canada through Genome Canada and the Ontario Genomics Institute (OGI-188). This research also received funding from the Italian Ministry for Education, University and Research (Ministero dell'Istruzione, dell'Università e della Ricerca - MIUR) PRIN2020 code 20203P8C3X to A.B.

Author Information

Conceptualization: G.M., M.M.A., A.Bou., B.S.; Data Curation: S.T., G.M., M.M.A., B.S.; Formal Analysis: K.K., M.A.L., R.R., S.H., H.M., B.S.; Investigation: K.K., M.O.M., A.Bro., M.L.T., E.Z.-H., E.H.G., L.V., A.Bru., E.S., M.P., S.D.A., E.S.-A., A.Bou., A.M., D.C., S.T., B.S.; Methodology; K.K., M.A.L., A.Bou., B.S.; Project Administration: B.S., A.Bou., H.M.; Supervision: M.M.A., A.Bou., B.S.; Validation; K.K., M.O.M.; Visualization; K.K., M.O.M.; Writing-original draft: K.K., M.O.M.; Writing-review and editing: S.T., A.Bru., A.Bou., M.M.A., B.S.

Ethics Declaration

The study protocol was approved by the Western University Research Ethics Board (REB 106302). Informed consent was obtained from participating cases or their guardians; the study was approved by the Internal Ethics Committee of the participating units, in accordance with the Declaration of Helsinki. All samples and records were de-identified.

Conflict of Interest

Bekim Sadikovic is a shareholder in EpiSign Inc., a biotech company involved in commercialization of EpiSign technology. All other authors declare no conflicts of interest.

Additional Information

The online version of this article (https://doi.org/10.1016/j.gim.2023.101041) contains supplementary material, which is available to authorized users.

Affiliations

[1]Verspeeten Clinical Genome Centre, London Health Sciences Centre, London, Canada; [2]Department of Clinical Genetics, Erasmus University Medical Center, Rotterdam, The Netherlands; [3]Department of Genetics, University of Groningen, University Medical Center Groningen, Groningen, The Netherlands; [4]Greenwood Genetic Center, Greenwood, SC; [5]Department of Human Genetics, Radboud University Medical Center, Nijmegen, The Netherlands; [6]Medical Genetics Unit, AOOR Villa Sofia-Cervello Hospitals, Palermo, Italy; [7]Department of Health Promotion, Mother and Child Care, Internal Medicine and Medical Specialties, University of Palermo, Palermo, Italy; [8]Pediatric Onco-Hematology, Regina Margherita Children's Hospital, Città della Salute e della Scienza di Torino, Torino, Italy; [9]Department of Medical Sciences, University of Turin, Turin, Italy; [10]Immunogenetics and Transplant Biology Service, Città della Salute e della Scienza University Hospital, Turin, Italy; [11]Department of Public Health and Pediatrics, University of Turin, Turin, Italy; [12]Department of Endocrinology and Genetics, University Clinic for Children's Diseases, Medical Faculty, University Sv. Kiril i Metodij, Skopje, North Macedonia; [13]Medical Genetics Unit, Città della Salute e della Scienza University Hospital, Turin, Italy; [14]Laboratory of Regulatory and Functional Genomics, Fondazione IRCCS Casa Sollievo della Sofferenza, San Giovanni Rotondo (Foggia), Italy; [15]Department

of Molecular Medicine and Medical Biotechnology, University of Naples Federico II, Naples, Italy; [16]Amsterdam UMC, University of Amsterdam, Department of Human Genetics, Amsterdam Reproduction and Development Research Institute, Amsterdam, The Netherlands; [17]Department of Pathology and Laboratory Medicine, Western University, London, Canada

References

1. Hui TYJ, Burt A. Estimating linkage disequilibrium from genotypes under Hardy-Weinberg equilibrium. *BMC Genet*. 2020;21(1):21. http://doi.org/10.1186/s12863-020-0818-9
2. Kvarnung M, Nordgren A. Intellectual disability and rare disorders: a diagnostic challenge. *Adv Exp Med Biol*. 2017;1031:39-54. http://doi.org/10.1007/978-3-319-67144-4_3
3. Schübeler D. Function and information content of DNA methylation. *Nature*. 2015;517(7534):321-326. http://doi.org/10.1038/nature14192
4. Cooper DN, Mort M, Stenson PD, Ball EV, Chuzhanova NA. Methylation-mediated deamination of 5-methylcytosine appears to give rise to mutations causing human inherited disease in CpNpG trinucleotides, as well as in CpG dinucleotides. *Hum Genomics*. 2010;4(6):406-410. http://doi.org/10.1186/1479-7364-4-6-406
5. Velasco G, Francastel C. Genetics meets DNA methylation in rare diseases. *Clin Genet*. 2019;95(2):210-220. http://doi.org/10.1111/cge.13480
6. Aref-Eshghi E, Rodenhiser DI, Schenkel LC, et al. Genomic DNA methylation signatures enable concurrent diagnosis and clinical genetic variant classification in neurodevelopmental syndromes. *Am J Hum Genet*. 2018;102(1):156-174. http://doi.org/10.1016/j.ajhg.2017.12.008
7. Gregor A, Oti M, Kouwenhoven EN, et al. De novo mutations in the genome organizer CTCF cause intellectual disability. *Am J Hum Genet*. 2013;93(1):124-131. http://doi.org/10.1016/j.ajhg.2013.05.007
8. Bastaki F, Nair P, Mohamed M, et al. Identification of a novel CTCF mutation responsible for syndromic intellectual disability – a case report. *BMC Med Genet*. 2017;18(1):68. http://doi.org/10.1186/s12881-017-0429-0
9. Hori I, Kawamura R, Nakabayashi K, et al. CTCF deletion syndrome: clinical features and epigenetic delineation. *J Med Genet*. 2017;54(12):836-842. http://doi.org/10.1136/jmedgenet-2017-104854
10. Chen F, Yuan H, Wu W, et al. Three additional de novo CTCF mutations in Chinese patients help to define an emerging neurodevelopmental disorder. *Am J Med Genet C Semin Med Genet*. 2019;181(2):218-225. http://doi.org/10.1002/ajmg.c.31698
11. Wang T, Hoekzema K, Vecchio D, et al. Large-scale targeted sequencing identifies risk genes for neurodevelopmental disorders. *Nat Commun*. 2020;11(1):4932. http://doi.org/10.1038/s41467-020-18723-y
12. Hiraide T, Yamoto K, Masunaga Y, et al. Genetic and phenotypic analysis of 101 patients with developmental delay or intellectual disability using whole-exome sequencing. *Clin Genet*. 2021;100(1):40-50. http://doi.org/10.1111/cge.13951
13. Valverde de Morales HG, Wang HV, Garber K, Cheng X, Corces VG, Li H. Expansion of the genotypic and phenotypic spectrum of CTCF-related disorder guides clinical management: 43 new subjects and a comprehensive literature review. *Am J Med Genet A*. 2023;191(3):718-729. http://doi.org/10.1002/ajmg.a.63065
14. Konrad EDH, Nardini N, Caliebe A, et al. CTCF variants in 39 individuals with a variable neurodevelopmental disorder broaden the mutational and clinical spectrum. *Genet Med*. 2019;21(12):2723-2733. http://doi.org/10.1038/s41436-019-0585-z
15. Richards S, Aziz N, Bale S, et al. Standards and guidelines for the interpretation of sequence variants: a joint consensus recommendation of the American College of Medical Genetics and Genomics and the Association for Molecular Pathology. *Genet Med*. 2015;17(5):405-424. http://doi.org/10.1038/gim.2015.30
16. Nykamp K, Anderson M, Powers M, et al. Sherloc: a comprehensive refinement of the ACMG-AMP variant classification criteria. *Genet Med*. 2017;19(10):1105-1117. http://doi.org/10.1038/gim.2017.37
17. Aref-Eshghi E, Bend EG, Colaiacovo S, et al. Diagnostic utility of genome-wide DNA methylation testing in genetically unsolved individuals with suspected hereditary conditions. *Am J Hum Genet*. 2019;104(4):685-700. http://doi.org/10.1016/j.ajhg.2019.03.008
18. Aryee MJ, Jaffe AE, Corrada-Bravo H, et al. Minfi: a flexible and comprehensive Bioconductor package for the analysis of Infinium DNA methylation microarrays. *Bioinformatics*. 2014;30(10):1363-1369. http://doi.org/10.1093/bioinformatics/btu049
19. Aref-Eshghi E, Kerkhof J, Pedro VP, et al. Evaluation of DNA methylation episignatures for diagnosis and phenotype correlations in 42 Mendelian neurodevelopmental disorders. *Am J Hum Genet*. 2020;106(3):356-370. http://doi.org/10.1016/j.ajhg.2020.01.019
20. Ho DE, Imai K, King G, Stuart EA. Matching as nonparametric preprocessing for reducing model dependence in parametric causal inference. *Polit Anal*. 2007;15(3):199-236. http://doi.org/10.1093/pan/mpl013
21. Ritchie ME, Phipson B, Wu D, et al. limma powers differential expression analyses for RNA-sequencing and microarray studies. *Nucleic Acids Res*. 2015;43(7):e47. http://doi.org/10.1093/nar/gkv007
22. Houseman EA, Accomando WP, Koestler DC, et al. DNA methylation arrays as surrogate measures of cell mixture distribution. *BMC Bioinformatics*. 2012;13(1):86. http://doi.org/10.1186/1471-2105-13-86
23. Benjamini Y, Hochberg Y. Controlling the false discovery rate: a practical and powerful approach to multiple testing. *J R Stat Soc B (Methodol)*. 1995;57(1):289-300. http://doi.org/10.1111/j.2517-6161.1995.tb02031.x
24. Levy MA, Relator R, McConkey H, et al. Functional correlation of genome-wide DNA methylation profiles in genetic neurodevelopmental disorders. *Hum Mutat*. 2022;43(11):1609-1628. http://doi.org/10.1002/humu.24446
25. Gu Z, Gu L, Eils R, Schlesner M, Brors B. circlize implements and enhances circular visualization in R. *Bioinformatics*. 2014;30(19):2811-2812. http://doi.org/10.1093/bioinformatics/btu393
26. Peters TJ, Buckley MJ, Statham AL, et al. De novo identification of differentially methylated regions in the human genome. *Epigenetics Chromatin*. 2015;8(1):6. http://doi.org/10.1186/1756-8935-8-6
27. Cavalcante RG, Sartor MA. annotatr: genomic regions in context. *Bioinformatics*. 2017;33(15):2381-2383. http://doi.org/10.1093/bioinformatics/btx183
28. Phipson B, Maksimovic J, Oshlack A. missMethyl: an R package for analyzing data from Illumina's HumanMethylation450 platform. *Bioinformatics*. 2016;32(2):286-288. http://doi.org/10.1093/bioinformatics/btv560
29. Dehingia B, Milewska M, Janowski M, Pękowska A. CTCF shapes chromatin structure and gene expression in health and disease. *EMBO Rep*. 2022;23(9):e55146. http://doi.org/10.15252/embr.202255146
30. Franco MM, Prickett AR, Oakey RJ. The role of CCCTC-binding factor (CTCF) in genomic imprinting, development, and Reproduction. *Biol Reprod*. 2014;91(5):125. http://doi.org/10.1095/biolreprod.114.122945
31. Chao W, Huynh KD, Spencer RJ, Davidow LS, Lee JT. CTCF, a candidate trans-acting factor for X-inactivation choice. *Science*. 2002;295(5553):345-347. http://doi.org/10.1126/science.1065982
32. Shukla S, Kavak E, Gregory M, et al. CTCF-promoted RNA polymerase II pausing links DNA methylation to splicing. *Nature*. 2011;479(7371):74-79. http://doi.org/10.1038/nature10442
33. Wang H, Maurano MT, Qu H, et al. Widespread plasticity in CTCF occupancy linked to DNA methylation. *Genome Res*. 2012;22(9):1680-1688. http://doi.org/10.1101/gr.136101.111
34. Vietri Rudan M, Barrington C, Henderson S, et al. Comparative Hi-C reveals that CTCF underlies evolution of chromosomal domain architecture. *Cell Rep*. 2015;10(8):1297-1309. http://doi.org/10.1016/j.celrep.2015.02.004
35. Debaugny RE, Skok JA. CTCF and CTCFL in cancer. *Curr Opin Genet Dev*. 2020;61:44-52. http://doi.org/10.1016/j.gde.2020.02.021

36. Damaschke NA, Gawdzik J, Avilla M, et al. CTCF loss mediates unique DNA hypermethylation landscapes in human cancers. *Clin Epigenetics*. 2020;12(1):80. http://doi.org/10.1186/s13148-020-00869-7
37. Saldaña-Meyer R, Rodriguez-Hernaez J, Escobar T, et al. RNA interactions are essential for CTCF-mediated genome organization. *Mol Cell*. 2019;76(3):412-422.e5. http://doi.org/10.1016/j.molcel.2019.08.015
38. Hashimoto H, Wang D, Horton JR, Zhang X, Corces VG, Cheng X. Structural basis for the versatile and methylation-dependent binding of CTCF to DNA. *Mol Cell*. 2017;66(5):711-720.e3. http://doi.org/10.1016/j.molcel.2017.05.004
39. Pugacheva EM, Kubo N, Loukinov D, et al. CTCF mediates chromatin looping via N-terminal domain-dependent cohesin retention. *Proc Natl Acad Sci U S A*. 2020;117(4):2020-2031. http://doi.org/10.1073/pnas.1911708117
40. Helsmoortel C, Vulto-van Silfhout AT, Coe BP, et al. A SWI/SNF-related autism syndrome caused by de novo mutations in ADNP. *Nat Genet*. 2014;46(4):380-384. http://doi.org/10.1038/ng.2899
41. Van Dijck A, Vulto-van Silfhout AT, Cappuyns E, et al. Clinical presentation of a complex neurodevelopmental disorder caused by mutations in ADNP. *Biol Psychiatry*. 2019;85(4):287-297. http://doi.org/10.1016/j.biopsych.2018.02.1173
42. Sun X, Yu W, Li L, Sun Y. ADNP controls gene expression through local chromatin architecture by association with BRG1 and CHD4. *Front Cell Dev Biol*. 2020;8:553. http://doi.org/10.3389/fcell.2020.00553
43. Kaaij LJT, Mohn F, van der Weide RH, de Wit E, Bühler M. The ChAHP complex counteracts chromatin looping at CTCF sites that emerged from SINE expansions in mouse. *Cell*. 2019;178(6):1437-1451.e14. http://doi.org/10.1016/j.cell.2019.08.007
44. Hussen DF, Kamel AK, Mekkawy MK, Ashaat EA, El Ruby MO. Phenotypic and molecular cytogenetic analysis of a case of monosomy 1p36 syndrome due to unbalanced translocation. *Mol Syndromol*. 2020;11(5-6):284-295. http://doi.org/10.1159/000510428
45. Gajecka M, Mackay KL, Shaffer LG. Monosomy 1p36 deletion syndrome. *Am J Med Genet C Semin Med Genet*. 2007;145C(4):346-356. http://doi.org/10.1002/ajmg.c.30154
46. Angelopoulou E, Paudel YN, Shaikh MF, Piperi C. Flotillin: a promising biomarker for Alzheimer's disease. *J Pers Med*. 2020;10(2):20. http://doi.org/10.3390/jpm10020020
47. Swanwick CC, Shapiro ME, Vicini S, Wenthold RJ. Flotillin-1 promotes formation of glutamatergic synapses in hippocampal neurons. *Dev Neurobiol*. 2010;70(13):875-883. http://doi.org/10.1002/dneu.20828
48. Kawarai T, Tajima A, Kuroda Y, et al. A homozygous mutation of VWA3B causes cerebellar ataxia with intellectual disability. *J Neurol Neurosurg Psychiatry*. 2016;87(6):656-662. http://doi.org/10.1136/jnnp-2014-309828
49. Jalali A, Bassuk AG, Kan L, et al. HeyL promotes neuronal differentiation of neural progenitor cells. *J Neurosci Res*. 2011;89(3):299-309. http://doi.org/10.1002/jnr.22562